SEMARAK ILMU PUBLISHING

CFD Letters

Journal homepage:
https://semarakilmu.com.my/journals/index.php/CFD_Letters/index
ISSN: 2180-1363

Aerodynamic Characterization of Darrieus Turbines during Self-Start at different Azimuthal Quadrants

Shaza Rae Selvarajoo[1], Zulfaa Mohamed-Kassim[1,*], Wei Shyang Chang[1]

[1] School of Aerospace Engineering, Universiti Sains Malaysia, 14300, Nibong Tebal, Penang, Malaysia

ARTICLE INFO

Article history:
Received 4 August 2022
Received in revised form 8 September 2022
Accepted 12 October 2022
Available online 1 February 2023

Keywords:
Vertical-axis turbines; Darrieus turbines; Self-starting; Transient flows; Rotor torque; Torque breakdown

ABSTRACT

One key technology to extract kinetic energy from wind and water is the vertical-axis turbines. However, these flows and currents often fluctuate, forcing the turbine rotors to operate in transient modes. To improve rotor performance, the transient aerodynamic characteristics across the four quadrants of the rotor sweep must be well-understood. We address this need by simulating the transient process of a 3-bladed Darrieus turbine rotor during self-start using the dedicated turbine aerodynamics software QBlade. The simulated transient evolution of the rotor compares well against the experimental and computational-fluid-dynamics data from previous studies. When the rotor self-starts within its first three cycles, its torque is contributed differently from each of the four quadrants. Respectively, its windward and upwind quadrant positively contributes by up to 43% and 326% each to the overall torque, and the leeward and downwind quadrant negatively reduces by up to -346% and -85% each from the overall torque. However, upon reaching steady state, these roles change where the positive torques are contributed by the upwind and leeward quadrants by up to 120% and 10%, respectively, while the negative torques are caused by the downwind and windward quadrants by up to -18% and -13%, respectively. Insights into these rotor dynamics can be later used to propose newer rotor designs or operations to improve the transient performance of the turbine.

1. Introduction

Rising demand in energy, projected to increase by more than 40% [1] within the next 30 years, and will remain as one of the key contributors to climate change which ultimately leads to global warming. The use of alternative forms of energy are thus necessary to address this issue, particularly those from renewable and sustainable sources. In this context, the energy extracted from wind globally has seen the largest annual growth recently, of about 14% in 2020, compared to those from other renewable sources [2]. A key technology to extract wind energy is the vertical-axis turbine. The designs of these systems can be adopted to extract hydrokinetic energy from water streams, e.g., from river flows or ocean currents. There are several features of vertical-axis turbines, particularly on the practicality of their operation and cost effectiveness over their manufacturing and

* *Corresponding author.*
E-mail address: zulfaa@usm.my (Zulfaa Mohamed-Kassim)

https://doi.org/10.37934/cfdl.15.2.126142

maintenance processes. With regards to their operation, the biggest advantage is their omnidirectionality in receiving flows from any direction, especially those that are subjected to large amounts of fluctuations or frequent flow reversals [3]. The omnidirectional capability of the vertical-axis turbines makes them particularly suitable for operations in built environments and urban areas [3–5] that are continuously exposed to fluctuating wind conditions, as well as in coastal oceans that are subjected to cyclical tidal currents [6]. Furthermore, the transmission systems for wind turbines can be placed on the ground, thus reducing their manufacturing complexity and maintenance cost; those for the hydrokinetic turbines can be placed above the water surface on floating platforms to avoid submerging their electrical components in water [3,7].

For vertical-axis turbines, there exists a tip-speed ratio (*TSR, or* λ) which is optimum, where power production and efficiency are optimized [8]. The transient aerodynamics of Darrieus-type presents an important aspect of Darrieus rotor operations; the nature of unsteady loading conditions [9,10] will by default, imply that the rotor is frequently in a transient operation mode and thus, it will stray from the optimum tip speed ratio (λ), decreasing the efficiency of the system. The difficulty with transient aerodynamics lies in its complexity. There are two types of transient operations for a Darrieus turbine: deceleration and self-starting. Indeed, these scenarios can happen concurrently or successively. The self-starting mode is the focus of this work. A recent definition of self-starting according to Worasinchai *et al.,* [11] is that the rotor is deemed self-starting if it could accelerate from rest to the λ where thrust was continuously generated over the Darrieus flight path. However, Darrieus turbines are known to face difficulty when self-starting due to low starting torque production [12].

Because of the low self-starting torque, many studies have devoted attention to improving the self-starting capability and have identified key design parameters which can improve self-starting. One of the main parameters is static airfoil pitch, studied by previous researchers [13–17]. These studies found that pitching angles significantly improve the self-starting capabilities of lift driven vertical-axis rotors. Pitching the individual rotor blades optimises the angle of attack (α), which increases the lift generated by the blades. The increased lift leads to additional torque, and thus improved self-starting. Changing the airfoil profiles were also attempted by several researchers, [13,17–22]. Indeed, it was shown that there is an optimum solidity and airfoil profile for self-starting. Specifically, cambered airfoils are better for self-starting due to greater torque generation. Regarding the solidity studied by previous researchers [16,13,21–23]. When viewing a rotor cross section, solidity is the ratio between the cross-sectional area occupied by the blades to the rotor cross sectional area. In short, solidity is a measure of how the air is squeezed through the rotor. Concurrently, Du [13] experimentally showed that increasing the solidity resulted in the increase of curvature effects. Specifically, these curvature effects create a virtual camber of the airfoil rotor blades. If the airfoil is already cambered, the virtual camber exaggerates the camber even further. The increased curvature effects lead to reduced blade incidence angles (α), thus, delays rotor blade stall and improves the performance at lower λ. However, cambered airfoil stalls are delayed and prematurely experienced when encountering positive and negative α respectively. Thus, an increase in camber may be a drawback if negative α are encountered. Essentially, solidity and airfoil profiles ultimately influence the flow α, thus altering the lift generated, and consequently the rotor performance.

Design changes by turbine designers must know where, when, and how to implement them. A method to simplify the rotor geometry is to split them into quadrants, following the work by Rezaeiha *et al.,* [24], where the rotor is split, according to the azimuthal angle (θ), into the upwind (defined by $45^\circ \leq \theta < 135^\circ$), leeward ($135^\circ \leq \theta < 225^\circ$), downwind ($225^\circ \leq \theta < 315^\circ$) and windward quadrants ($315^\circ \leq \theta < 45^\circ$). Splitting the rotor into these quadrants bring insights into which quadrant provides the

most torque. Consequently, the control strategies can be applied to the respective quadrants which perform poorly.

A quadrant breakdown for steady state a Darrieus rotor has been performed by Rezaeiha *et al.,* [24]. However, a quadrant breakdown for a self-starting rotor is not yet covered in literature. Elucidating the physics of the quadrants during self-start, by analysing the behaviour and torque-contribution of each quadrant, will allow designers to focus their strategies for improvements in those quadrants. Thus, the present study is aimed at elucidating the performance of each rotor quadrant during self-start, such that quadrant-wise design changes can be recommended. In this respect, the objective of the study is to numerically simulate a H-Darrieus rotor and investigate the performance of the rotor within the four quadrants during self-start.

2. Methodology

2.1 Turbine Model

A three-bladed H-Darrieus rotor was simulated numerically in this work, based on the same rotor studied experimentally by Rainbird [25]. The rotor was selected because it had been used as a reference to study Darrieus rotors in several studies, thus providing sufficient data to be used for validation and comparison. Table 1 lists the physical properties of the rotor along with its tower and operational parameters.

Table 1
Rotor properties and other relevant parameters

Rotor Properties		Tower and Operational Parameters	
Blade Profile	NACA 0018	Tower Height (m)	2
Chord Length (mm)	83	Tower Central Axis Top Radius (mm)	40
Span (m)	1	Tower Central Axis Bot Radius (mm)	40
Rotor Axis Diameter (mm)	40	Tower Drag Coefficient	0.5
Rotor Radius (mm)	375	Initial Rotor Speed (rad/s)	0
Moment of Inertia (kg.m^2)	0.018	Velocity inflow (m/s)	6

2.2 Numerical Model

The flow dynamics surrounding the rotor during self-start was modelled using the non-linear lifting-line and free-vortex-wake (NLLFVW) formulations, derived from the work by Van Garrel [26] and packaged in the open-source turbine aerodynamics software QBlade [27]. The software includes a GUI environment to seamlessly design and simulate three-dimensional (3D) turbine rotors with detailed specifications to operate within realistic environments, and has been validated against experimental results [28–32].

The transient evolution of the rotor torque (T) is computed from the aerodynamic forces on the blades based on the polar data of lift and drag coefficients (C_L and C_D) of the NACA 0018 airfoil (see Figure 1) and the relative velocity (V_{rel}) and the angle of attack (α) of the blade. These two blade parameters are vectorially resolved from the free-stream velocity V_∞, the blade velocity V_b, and the induced velocities V_{ind}, which in turn are influenced by bounded vortex elements that represent the blades as lifting surfaces through the Biot-Savart Law as shown in Eq. (1). Vortex elements that represent the shed wakes downstream of the blades are included as well in determining the induced velocities.

The lifting-line formulation within QBlade iteratively computes the flow circulations (Γ) of these vortex elements, based on the airfoil polar data via the Kutta-Joukowski Theorem as shown in Eq. (2),

until the computed values converge at each stepsize. The forces on the blades are then computed based on the converged C_L and C_D values, after which the rotor (whose inertia is I) is stepped forward in time at a rotational angular velocity of $\dot{\omega}$ through Eq. (3). At the end of each stepsize, wakes are shed behind the trailing edges of the blades, convecting new vortex elements downstream within the simulation. The flow circulations for these trailing and shed vortex elements are computed through the Kutta condition as given in Eqs. (4) and (5).

$$V_{ind} = -\frac{1}{4\pi}\int \Gamma \frac{\vec{r}\times\partial\Gamma}{r^3} \tag{1}$$

$$\partial C_L(\alpha) = \rho V_{rel} \times \partial\Gamma \tag{2}$$

$$\dot{\omega} = \frac{T}{I} \tag{3}$$

$$\Gamma_{trail} = \frac{\partial\Gamma_{bound}}{\partial x}\Delta x \tag{4}$$

$$\Gamma_{shed} = \frac{\partial\Gamma_{bound}}{\partial x}\Delta t \tag{5}$$

The airfoil polar data used in this iterative process is pre-determined within QBlade from the XFLR5 calculation tool for the pre-stall region [33] based on the free-stream Reynolds number of 3,000 and 130,000 which represent the approximate lowest and highest *Re* acting on the airfoil. This range was obtained via up to 104 simulations with polar data varying by up to ± 15% of C_L and C_D values. These various polars were tested and it was found that the minimum and maximum *Re* were approximately similar despite the variation of the input polars.

Additionally, the computed polars were then extended beyond the stall region through the Montgomerie extrapolation model [34]. The local blade *Re* is computed at every timestep, which is then used to linearly interpolate between $3{,}000 \leq Re \leq 130{,}000$ to obtain the correct C_L and C_D at the local *Re*. This process is performed to accurately simulate real airfoils, whose coefficients change depending on their *Re* values.

While rotating, the unsteady aerodynamic effect of dynamic stall influences the forces on the blades operating in the vicinity of their stall angles. This effect is modelled inside QBlade using the Beddoes-Leishman model [35].

The presented numerical model is applied from rest until steady-state and beyond. The TSR increases as the aerodynamic forces on the blades accelerate the rotor. Eventually, the TSR converges to a constant value which fluctuates by less than 0.1%, demarcating the beginning of the steady-state process. The time taken for the TSR to converge (t') is used to define a normalized time scale T^* defined as

$$T^* = \frac{t}{t'} \tag{6}$$

where t represents the real time at every timestep, with $T^* = 1$ denoting the beginning of the steady-state process. Beyond $T^* = 1$, the computation of the rotor dynamics is repeated as described above. Once the rotor is in the steady-state mode, the results do not change much beyond $T^* = 1$.

Essentially, simulations of Darrieus rotors within QBlade attempt to model their operations as dynamically and as realistically as possible by combining physical and empirical modelling and incorporating various dynamic and three-dimensional effects. The NLLFVW model iteratively determines, at every time step, the angle of attack and the lift and drag coefficients of the rotor blades, taking into account the vortices from their trailing edges that alter the flow downstream and the dynamic stall effect that alters the lift forces on the blades (compared to those on static rotors which do not experience dynamic stall). Vortex interactions with the ground and tower are included empirically in the simulations. Beyond these models and empirical considerations, the blades are subjected to rotational effects such as the centrifugal forces and the Coriolis effect – collectively modelled as the Himmeslkamp effect [36] – and the curvature effect on the airfoil camber; however, these rotational effects are not incorporated in this work (see Section 2.5). Results from QBlade simulations on several types of Darrieus rotors and operating conditions have been extensively validated by Marten *et al.,* [27–29,37] and Balduzzi *et al.,* [31].

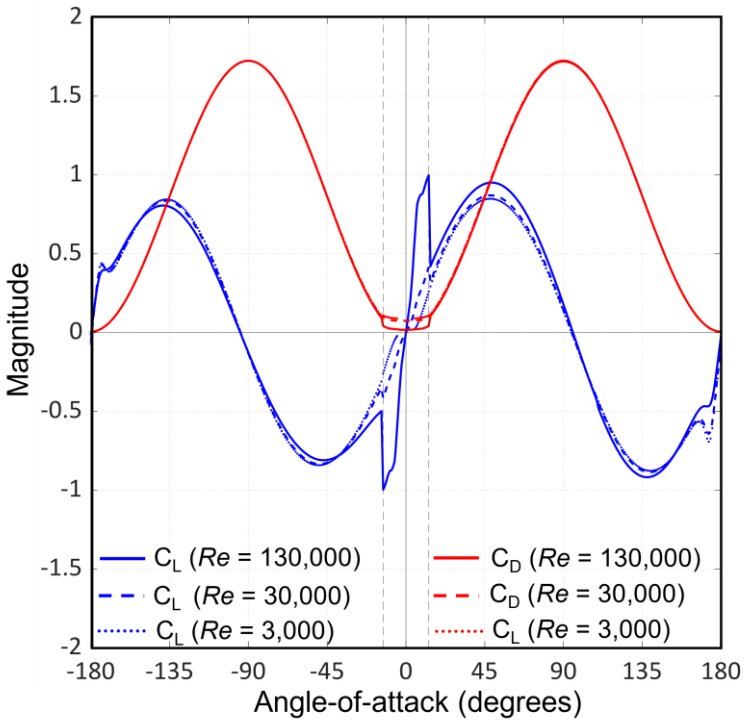

Fig. 1. The pre-determined tabulated polar data between $3000 \leq Re \leq 130{,}000$ using the XFLR5 tool and extrapolated beyond stall using the Montgomerie model embedded within QBlade. The $Re = 30{,}000$ polar is an example of an interpolated polar used in the simulation as Re changes.

2.3 Validation

The evolution of the TSR in the transient phase was simulated and compared with the experimental result of the same parameters by Rainbird [25] in Figure 2, along with the two-dimensional (2D) computational-fluid-dynamics (CFD) results by Zhu *et al.,* [16], Torabi *et al.,* [19], and Celik *et al.,* [38]. Differences between the TSR results from these simulations and that from the

experimental data (fitted with an 8th-degree polynomial) were evaluated, showing that the simulation from the present study produced the closest approximation to the real data with a mean error of 14% across the entire transient region, compared to 32.7%, 43.7%, and 96.5% for those by Zhu *et al.,* [16], Celik *et al.,* [38], and Torabi *et al.,* [19], respectively. In addition, the steady-state TSR is well-predicted by the QBlade simulation, off from the real data by 12%, compared to the errors of 9.2%, 24%, and 27.9 from the three CFD results (in the same order, respectively). Inaccuracies from these two-dimensional CFD simulations were likely to result from their inability to capture three-dimensional effects (e.g., blade-tip effect, flow asymmetries, vortical flows [39]) as well as real effects (e.g., interactions with the ground and tower). In contrast, the numerical model employed herein incorporates these effects through physical modelling and empirical data (e.g., vortex and dynamic-stall models, flow-structure interactions), with the added advantage of the considerably lower computational resources needed in the simulation, compared to that used in the CFD modelling.

The QBlade simulation differs the most from the real data during the "accelerated" phase of the transient process, where the rotor tip-speed accelerates from $0.75 \leq T^* \leq 0.9$; it predicts that the accelerated phase occurs earlier than that of the real data. Among the likely sources of errors are the lack of mechanical parasitic torque in the model, as well as the possible errors in the tabulated airfoil polar, especially within the extrapolated region beyond the stall [34]. In addition, QBlade cannot accurately capture the fine details of boundary layer separation because the airfoil is modelled as a one-dimensional lifting line. Nevertheless, the results produced by QBlade in this study is sufficiently reliable to characterize the rotor dynamics at various regions and stages of the transient process, based on comparisons with other studies (as stated in Section 3).

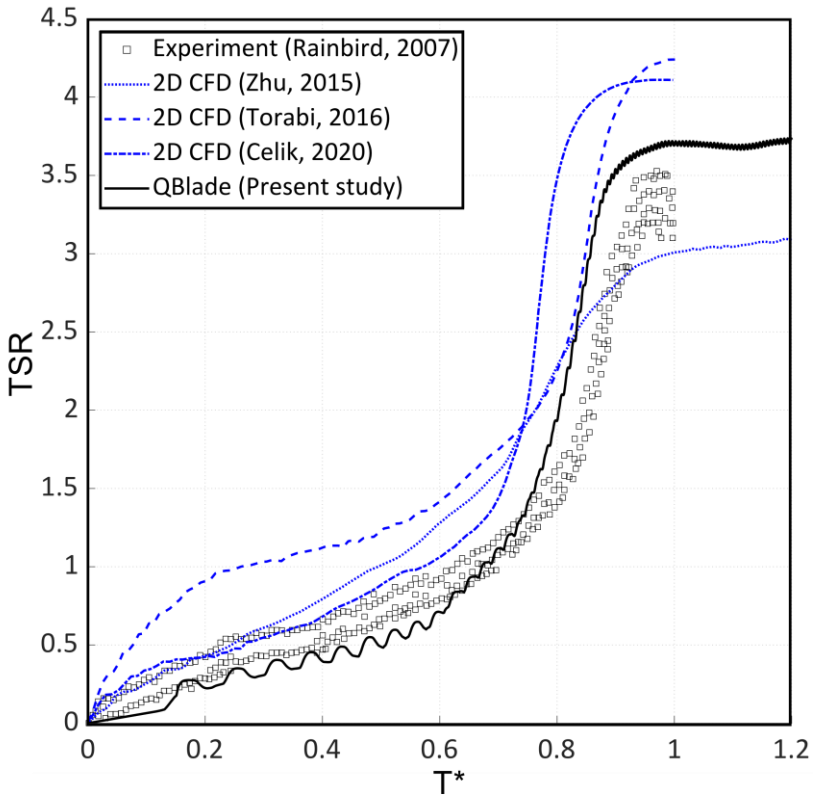

Fig. 2. Evolution of the TSR during self-starting: comparison between the QBlade simulation from the present study and the experimental and CFD results from previous works.

2.4 Reliability

To ensure the QBlade simulations converged reliably, the grid and time-step independence tests were performed with certain ranges of input parameters as listed in Table 2. The number of nodes represents the spatial discretization of the blade, the wake truncation represents the length of wake being simulated (to conserve computational resources), the wake concatenation represents the grouping of multiple vortex nodes into a single node (to accelerate simulation time, as described by Marten *et al.,* [29]), and the azimuthal step size ($\Delta\theta$) represents the time step.

The influence of the step size on the convergence error and simulation time in the present study is illustrated in Figure 3. The convergence error at any step size is defined as the mean error in the TSR values across the entire transient process (i.e., from start to steady state) predicted at that respective $\Delta\theta$ and those predicted at a reference $\Delta\theta$ of 1.5°. The reference step size chosen was the smallest one possible within the limits of the available computational resource, without having the simulation crashed. A time-step independence test was initially performed with 1.5° step size, 14 blade nodes, 4 revolution wake truncations, and 1 revolution wake concatenation, producing a mean error of 15% (measured between its transient TSRs against those from the experimental data). This error increased slightly by 0.5% when $\Delta\theta = 2°$, but surged to almost 3% when $\Delta\theta = 2.5°$ and to about 5% when $\Delta\theta = 3°$. For the actual simulation, a $\Delta\theta$ of 2° with 18 nodes were chosen that offered a suitably balance between computational fidelity and simulation time. The finer 18 blade nodes (instead of 14) compensates for the coarser 2° step-size (compared to 1.5°) to reduce the mean error from 15% to 14%.

Additionally, the previously mentioned 104 preliminary simulations demonstrated that as long as the rotor self-starts, all the features of self-starting (such as the lift peaks) are always present even with a polar variation of ±15% C_L and C_D, where the difference lays in the magnitudes of the features. Thus, absolute accuracy of polars to experimental polars is not a primary requirement in this study.

Table 2
Parameters selected for convergence testing

	Convergence test range	Selected parameter
Number of nodes (Nodes)	2 – 21	18
Wake truncation (Revolutions)	3 – 8	4
Wake concatenation (Revolutions)	0.5 – 4	1
Azimuthal Step size (Degrees)	1 – 5	2

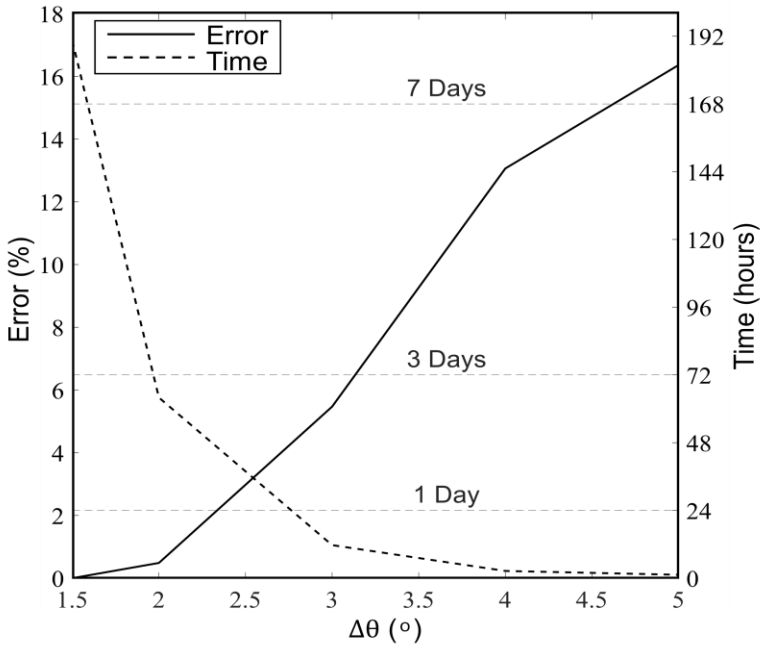

Fig. 3. Convergence errors and simulation times for different step sizes in the QBlade simulation of the present study, with the errors computed as the mean errors in TSRs across the transient process predicted at the respective $\Delta\theta$ and at $\Delta\theta$ =1.5°

2.5 Limitations

One limitation of the study was the lack of a parasitic mechanical torque, as experienced in the experimental setup due to the frictions in the bearing and generator. This effect decreased the rotor torque measured in the experiment and resulted in a smaller TSR when compared against the simulated one (as shown in Figure 2).

Another limiting factor is that the rotational effects are not modeled for vertical-axis turbines inside the version of QBlade (v.0.96.3) being used within this work; these are the curvature effect (which simulates a rotating airfoil with a modified virtual camber [32]) and the Himmelskamp effect (which delays blade stall due to the Coriolis and centrifugal forces [36]). The virtual camber effect has been demonstrated [32] to affect the value of the turbine power coefficient by up to 10% at large TSR values. Nonetheless, these rotational effects are likely to have smaller influence on rotor simulations at the beginning of the self-starting phase, which is the primary focus of this work.

3. Results

3.1 Azimuthal Data

Figure 4 presents the rotor dynamics in detail, in terms of the azimuthal variations on the angles of attack α and the force coefficients C_L, C_D, and C_t acting on one of the rotor blades for its first four cycles as the rotor starts from rest. The static mean C_t of a single cycle, however, is computed based on the interpolated polar data and ignores the effects of unsteady aerodynamics. These cycles represent the crucial early stage of self-starting with low TSRs of $\lambda < 1$ and weak torques, consistent with its definition of "critical region" by Arab *et al.,* [40]. In this simulation, the rotor accelerates across the transient process until it reaches steady state approximately within 17.5 cycles.

A noticeable characteristic in Figure 4 is the widely fluctuating α, ranging from -180^o to 180^o in the first four cycles, due to the low TSR values of $\lambda < 1$, as observed by Hill *et al.,* [41] and Arab *et*

al., [40]. Furthermore, the α values in the upwind half of the rotor ($0^{\circ} \leq \theta \leq 180^{\circ}$) and in the downwind half ($180^{\circ} \leq \theta \leq 360^{\circ}$) are not equal (i.e., α is asymmetric across a vertical line going through $\theta = 180^{\circ}$) due to the vortices shed from the upwind half spilling into the downwind half. These vortices slightly affect the α values in the downwind half. At low TSRs, these effects are small which causes the α plot to look symmetric, consistent with the experimental work by Douak *et al.,* [15]. For example, in cycle 1 $\theta = 90^{\circ}$ and $\theta = 270^{\circ}$, the corresponding α are $\alpha = 78^{\circ}$ $\alpha = -67.5^{\circ}$ respectively. The corresponding aerodynamic forces on the blade depend on these angles, which cause the coefficients of C_L, C_D, and C_t to vary widely as well. Several unique features of the rotor dynamics appear in response to these fluctuating forces.

Firstly, in the windward and leeward quadrants, the lift coefficients peak beyond their expected C_L values for the angles of attack being experienced at those azimuthal locations (as labelled in Figure 4). These lift peaks exceed their tabulated post-stall values by up to 184%. This behaviour is attributed to the unsteady aerodynamic effect of dynamic stall that is generally present within the vicinity of the post-stall regions of a Darrieus blade at low TSR values [8]. Specifically, as the blade repeatedly stalls and recovers while rotating about its central axis, α rapidly fluctuates above and below the tabulated airfoil stall value, inducing the dynamic stall behaviour. With the additional lift from dynamic stall, the lift peak in the windward quadrant causes a small rise in C_t, with the azimuthal locations of its peak virtually maintained the same across cycles 1 to 4. On the contrary, the lift peak in the leeward quadrant causes a large dip in C_t due to the reverse orientation of lift acting on the blade. This large dip strongly influences the rotor behaviour in the cycles 1 – 3. Furthermore, the leeward lift peaks and C_t dips evolve dramatically across the cycles: by the fourth cycle, the leeward lift peak and C_t dip magnitudes reduce significantly.

These changes on the rotor dynamics between the third and fourth cycles are driven by the changes in α within the vicinity of the azimuthal locations (isolated by the dotted circles in cycles 3 and 4). The visible changes in α inside these isolated circles are due to slight changes in the blade tip-speed ratios. This observation is consistent with the findings by Baker [42], where slight accelerations can greatly influence α by up to 25% at low λ.

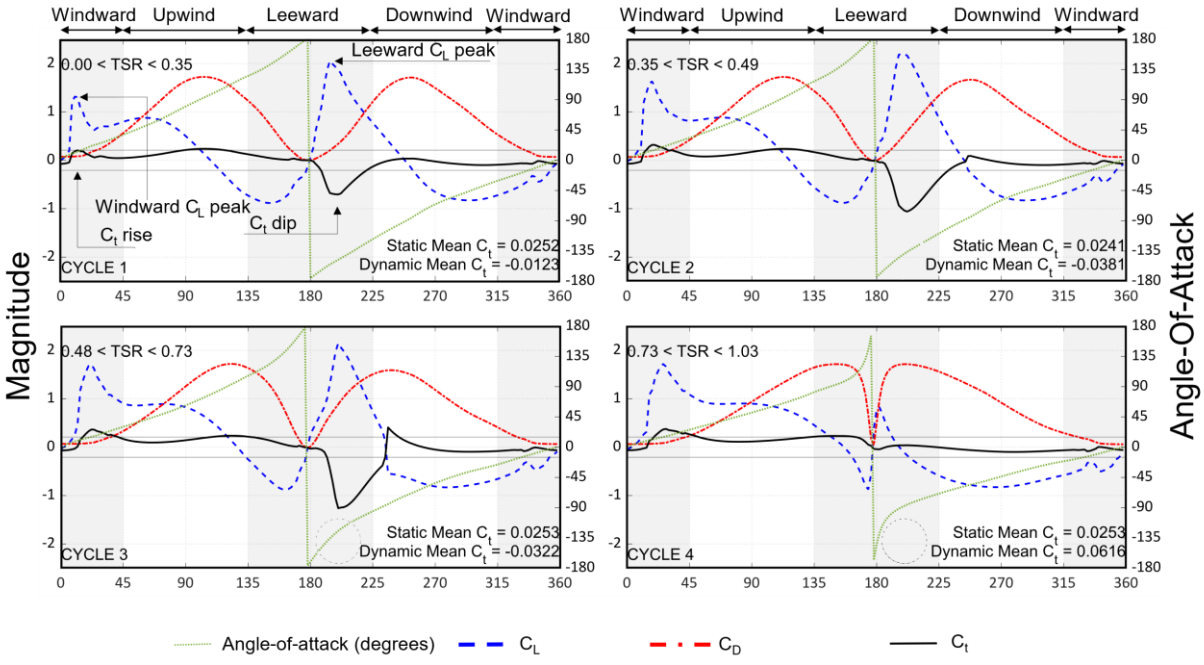

Fig. 4. Evolution of C_L, C_D, and C_t (left y-axis) and α (right y-axis) on a single reference blade in cycles 1 to 4 of the rotor during its self-start. Additionally, the static stall angle is $\pm 15^{\circ}$.

Figure 5 presents the rotor dynamics for cycles 5, 6, 8 and 11. Beyond cycle 11, these plots are relatively invariant as the rotor nears its steady-state operation. Generally, as the rotor cycle increases during its transient mode, its TSR accelerates, leading to the narrowing of the ranges of α; e.g., in cycle 11, the range narrows to $-6.3^{o} < \alpha < 10.6^{o}$. The continuous reduction of α range is consistent with the results obtained by Douak *et al.,* [15], Celik *et al.,* [38], and Arab *et al.,* [40]. The increased TSR causes the α range to reduce due to the orientation of the flow relative to the blade being dominated by the faster blade motion, rather than by the direction of the incoming freestream flow. Consequently, the smaller α range causes similar patterns of C_L, C_D, and C_t to be consistently reproduced across these later cycles (in contrast to those in cycles 1 – 4).

Furthermore, the windward and leeward lift peaks remain in Figure 5, with their magnitudes exceeding the tabulated polar by 216.4% due to dynamic stall, and the leeward peak having negative values. Both peaks coincide with the favourable rise in C_t values, due to the narrower ranges of α. In contrast, the leeward lift peak in cycles 1 to 4 produce negative C_t values due to the larger α ranges that extends to 180° at both ends.

The windward lift peak – consistent in magnitude across cycles 5,6,8 and 11 – is observed to slowly shift upwind towards $\theta = 90°$ as the cycle progresses, indicating that more torque is generated by the upwind region as the rotor approaches equilibrium (as discussed further in Section 3.2). The leeward lift peak, however, does not shift its azimuthal location but instead reduces continuously in magnitude. These lift peaks – as seen in Figure 4 and Figure 5 – are essential to the rotor dynamics as they govern the behaviour of the tangential force coefficients C_t that in turn determine the torque produced. These results extend the work by Celik *et al.,* [38] where specific aspects of the rotor dynamics can be elucidated, as discussed subsequently.

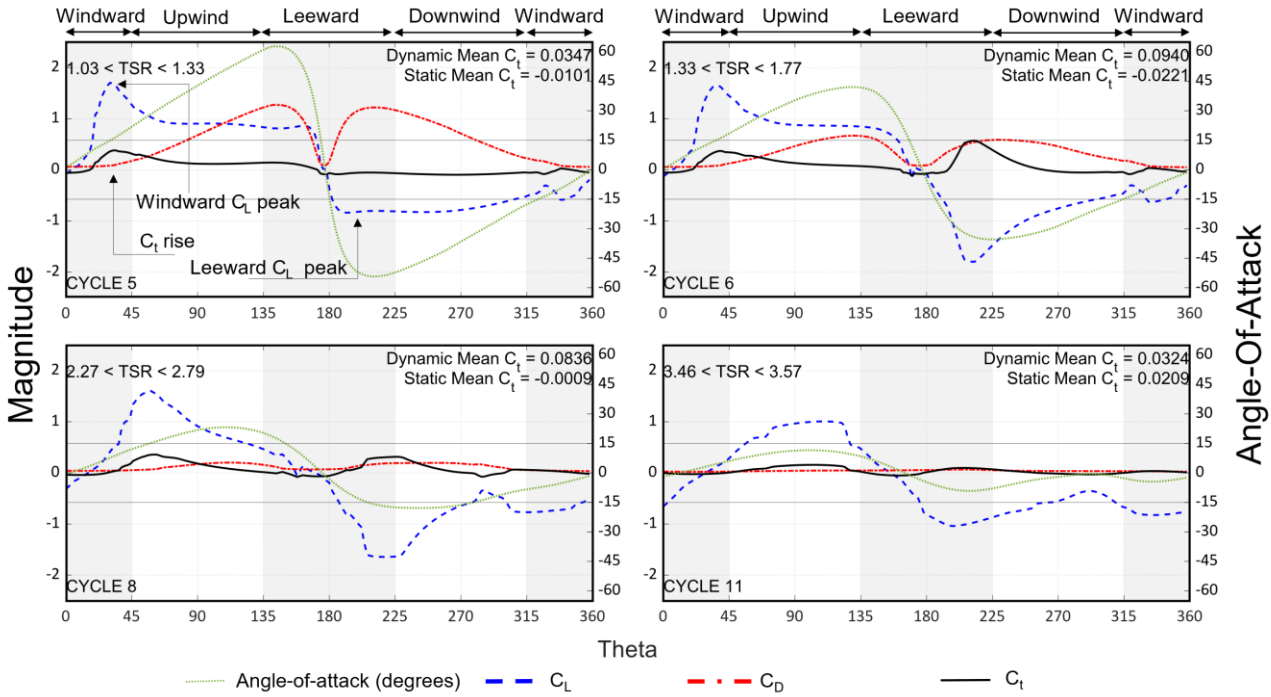

Fig. 5. Evolution of C_L, C_D, and C_t (left y-axis) and α (right y-axis) on a single reference blade in cycles 5 to 11 of the rotor during self-start. α is magnified by three-fold for clarify.

The key feature in elucidating self-starting rotors is the tangential force coefficient C_t, where greater C_t production leads to greater torque. The negative mean C_t from cycles 1 to 3 are found to emphasize how severely the lift peaks contribute to the self-starting. Furthermore, the mean cycle

C_t of cycle 3 is 200.6% smaller than that of cycle 11 (which has the smallest α range of all the cycles presented above). This low torque generated in cycles 1 – 3 are as expected at low TSR because H-Darrieus rotors have been known to experience difficulty in self-starting [41]. With regards to the windward lift peak, it contributes to a positive, albeit small C_t. The leeward lift peak, however, contributes significantly to negative C_t production, and is the reason why the mean C_t in cycles 1 to 3 are negative. Despite the negative values, they are not causing the rotor to decelerate because these values do not consider the contributions from the other two blades, which cumulatively, cause the mean torque coefficient to be positive. The positive mean torque accelerates the rotor and alters the magnitude of the leeward lift peak.

The increasing TSR strongly influences α, and thereby altering the leeward lift peak in cycles 3 and 4. Specifically, a local change of α by up to 35.5% (as labelled in the dotted circles), results in the reduction of the leeward lift peak by 61.5%, and ultimately mitigates the C_t dip magnitude by up to 103%. The results demonstrate how such a slight local change of α, at the right azimuthal locations, can be highly effective in mitigating negative C_t production, which is precisely why pitching can be so effective in self-starting, as demonstrated by Somoano & Huera-Huarte [43]. Lastly, the leeward peak evolves again in cycle 5 with higher TSR values of $\lambda \geq 1$ that causes reduction in the α range. The new α range of $\pm 90^{\circ}$ causes the lift to reverse and generate a C_t rise. Further analysis reveals that this is due to the vector orientations of the lift being significantly different between those in cycles 4 and 5. In cycles 1 to 3 (when $\lambda < 1$ and $-180^{\circ} \leq \alpha \leq +180^{\circ}$), the leeward lift peaks contribute parasitically because of the excessive α below -90° at the leeward quadrant, such that the magnitude of the lift is positive. It is found that a negative lift magnitude in the leeward quadrant is favourable, as evidenced by comparing the leeward C_t rise or dip due to the leeward lift peak in cycles 4 and 5 (see Figure 4). These results imply that the orientations of the lift vector are important and require further elucidation.

In cycles 5,6,8 and 11, with $\lambda > 1$, the smaller α range causes the rotor to consistently accelerate with positive cyclical mean C_t which implies that the smaller α range produces favourable combinations of lift and drag forces on the blades. The windward and leeward lift peaks, no longer evolving with respect to the subsequent cycles, contribute to the consistent positive cyclical mean C_t. The contribution of these peaks contrast with how the leeward lift peaks in cycles 1 to 3 coincides with the C_t dips.

This discussion presents the argument that α ranges below $\pm 90^{\circ}$ are favourable because it always generates positive mean C_t at every cycle, in contrast to those in cycles 1 to 3 which have α ranges of $\pm\ 180^{\circ}$ and generate cyclical mean torques that are negative. Specifically, the lower α ranges ensure that the leeward lift peaks (that is responsible for large dips in C_t in cycles 1 to 3) produce C_t peaks as well, thus generating greater cyclical mean C_t. For these reasons, lower α ranges are more favourable for torque generation in H-Darrieus rotors, and self-starting. Turbine designers will benefit from knowledge on how to precisely alter α such that it can improve self-starting. However, it is difficult to analyse the data in terms of azimuthal angles due to the large quantities of available data. Therefore, analysing the rotor dynamics in a more relevant manner is necessary, as presented in the following section.

3.2 Quadrant Data

The breakdown of torque contribution according to the quadrants are presented in Figure 6 following the quadrant breakdown by Rezaeiha *et al.,* [24], to characterize the self-starting performance of the rotor in an intuitive way. In the figure, there are four plots with each plot

representing a single quadrant. Each quadrant plot shows its respective torque contribution across self-starting.

For a single cycle, the sum of the four contributions equals ±100%. A sum resulting in -100%, then the net torque for that cycle is negative (occurring in cycles 1 – 3). Net negative torques do not imply that the rotor is decelerating, because it does not account for the contribution from the other blades. Next, individual bar chart values above or below ±100% represents overwork or underwork respectively.

In the figure, the windward quadrant contribution varies between positive and negative contribution. Positive contribution is mostly seen from cycles 1 – 13, while the rest of the cycles contribute negatively. This finding is due to the good combination of C_L and C_D in cycles 1 – 13, while a poor combination is experienced in the other cycles. Specifically, a good combination is usually $C_L > C_D$. Next, the upwind quadrant is vital to self-starting because it generates the majority of the self-starting and steady state torque. For example, the blade in the upwind during the first cycle generates up to 326% of C_t, and continuously generates large C_t contributions until steady-state (which contributes approximately 120% to C_t). Like the windward, the upwind generates large C_t due to the good combinations of lift and drag. This finding is also found in the work by Rezaeiha *et al.,* [24].

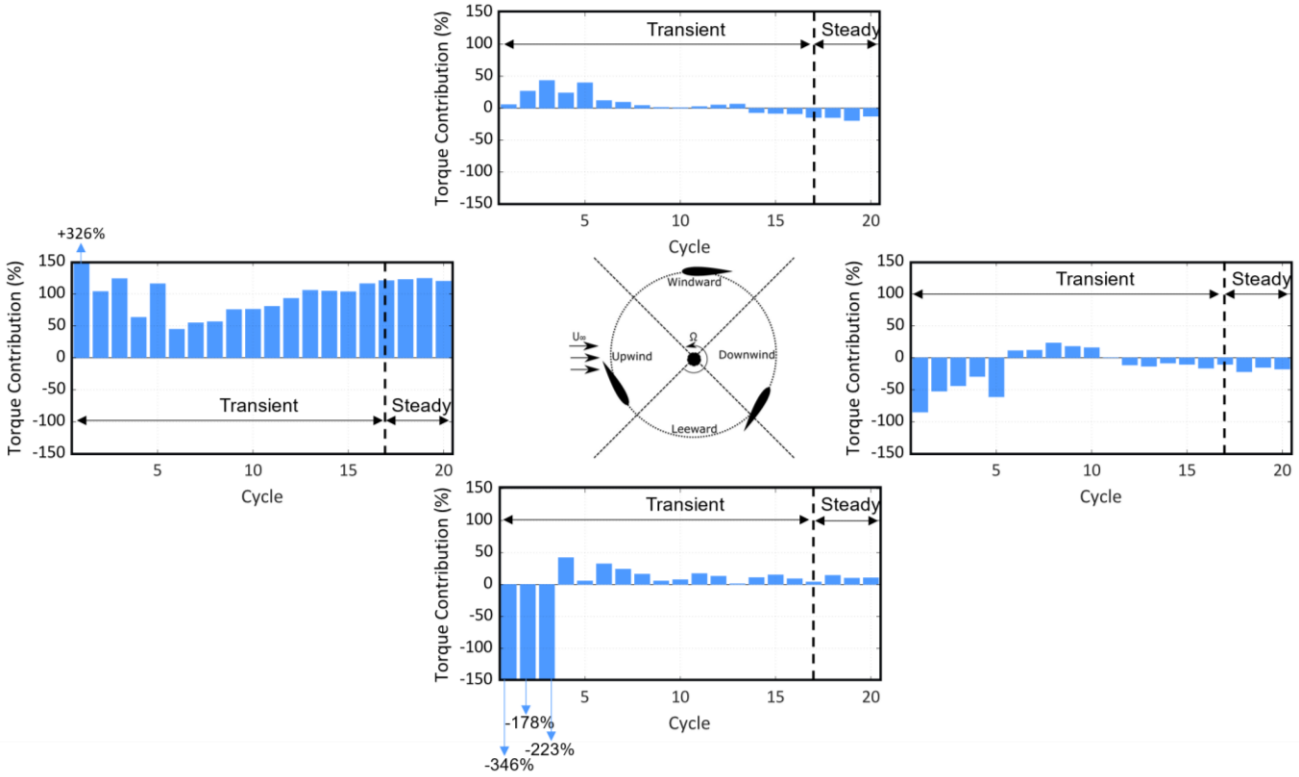

Fig. 6. Contribution of each quadrant to rotor torque per cycle (blue bars read from the left y-axis) and the cyclical and quadrant mean C_t (solid and dashed lines, respectively, read from the right y-axis). The breakdown is described by the diagram in the middle of the figure.

A key feature to note is the leeward quadrant, where the initial C_t contribution is strongly negative, especially within cycles 1 – 3 up to –346%, and is due to the leeward C_t dip. Eventually, as the TSR increases with cycle number, the contribution converts from negative to positive of approximately +10% at steady state (cycle 20). The downwind quadrant also experiences an initial negative contribution of -85% which turns positive in cycles 6 – 10 and contributes up to +16% to the cycle C_t. Eventually, the downwind stabilizes at -18% contribution at steady state. The alternating

fashion of the leeward and downwind contributions are due to the changing TSR, which affect α and thus directly influences the C_L and C_D combination.

C_L and C_D are key to elucidating the C_t contributions. C_t is positive in cycles 1 – 9 of the windward quadrant because it coincides with the windward C_L peak, shown in Figure 4. Because of the improved C_L due to dynamic stall, C_t in the windward quadrant is improved significantly. However, as TSR increases, this windward C_L peak shifts towards the upwind quadrant, shown in Figure 5. Therefore, the windward loses the advantage of dynamic stall and results in the quadrant producing negative C_t. The C_L peak shifts because as TSR increases, the α range reduces, and then α tends to exceed the static stall α only in the upwind shown clearly in cycle 9 of Figure 5. By exceeding static stall α in the upwind, dynamic stall thus occurs in that quadrant, which increases C_t.

Regarding the upwind quadrant, it constantly produces large C_t because of the combinations of C_L and C_D. In cycles 1 – 5 of Figure 4, a C_D peak is encountered; C_L is visibly smaller in comparison to C_D, yet such a large C_t is generated. Investigation reveals that the upwind second half ($90^\circ \leq \theta \leq 135^\circ$) is drag driven at this TSR, thus the C_D peak is an advantage. This finding is consistent with the work by Celik *et al.,* [38] which numerically investigates the same rotor, where it is found that the drag driven region can range between ($100^\circ \leq \theta \leq 250^\circ$) depending on the TSR.

As the TSR increases beyond 1, the upwind (and the whole rotor) becomes fully lift driven [38]. Additionally, C_D dramatically reduces and C_L rises. These features are evidenced in the cycles in Figure 5. Furthermore, the windward C_L peak shifts towards the upwind. These factors thus cause the upwind to contribute the most to C_t.

However, the leeward quadrant encounters the drawback of the drag driven nature of the rotor. Because the rotor is drag driven at low TSR, thus large C_D and small C_L is favourable. Since, the strong leeward C_L peak dominates the rotor forces in the cycles 1 – 3 in a "reversed orientation", the strong negative C_t dip exists. For this reason, the leeward quadrant contributes a large negative C_t. However, at cycles 6 and beyond, the existence of the leeward C_L peak causes the leeward C_t to become positive shown in Figure 5 due to the rotor being fully lift driven at TSRs above 1.

Lastly, the downwind quadrant begins and ends the self-starting process with negative C_t contributions due to the poor magnitude of C_L and a relatively larger C_D seen in cycles 2 – 5 of Figure 4 and cycles 11 and beyond in Figure 5. However, in the middle of self-starting, the downwind contribution of Figure 6 is positive for a few cycles. This effect elucidated by cycle 9 downwind quadrant of Figure 5 where it is shown that the relevant α at that TSR causes C_D to reduce, yet C_L remains high. Additionally, the leeward C_L peak extends slightly into the downwind quadrant. These features result in the temporary slight positive C_t contribution.

With the insights presented in this work, to improve self-starting, focus should be applied on improving α in the windward quadrant especially when TSR ≤ 1. An effective strategy is pitching, where it was shown by Zouzou *et al.,* [44] that pitching the blades of a Darrieus rotor with a TSR of 0.52 can significantly improve the total T output of the rotor. Specifically, pitching in the leeward quadrant by up to -40° can remove negative "T dips" in the rotor. An alternative method is via intra-cyclical control [45]. By actively accelerating the rotor during regions of poor performance (leeward quadrant), the TSR can be increased, and thus the α range can be decreased. In contrast, by decelerating the rotor at regions of good performance, α can be raised, which could be favourable in certain scenarios. An additional method is by creating a hybrid Darrieus-Savonius type rotor, which can take advantage of the drag driven leeward quadrant. Following the work by Mahrous [46], such a turbine has shown to mitigate the large T dip in the leeward quadrant at certain configurations. These methods of controlling α are good strategies to mitigating negative torque generation in the leeward quadrants.

Additional simulation data shows that the quadrant breakdown during the first few cycles in the downwind and windward is sensitive to the polar data used to perform the simulation. Physically, changes in the input polar data may be due to manufacturing defects, accumulation of dirt, icing, or deterioration of the blade. Therefore, caution is advised when attempting to improve the downwind and windward quadrants.

4. Conclusions

In this work, an investigation on the self-starting phase of a vertical-axis turbine was performed where the rotor experimented by Rainbird [25] was simulated. The simulation was performed using a combined lifting line theory and vortex wake model embedded inside QBlade, an open-source software dedicated for turbine simulations. Details of the physics of self-starting were presented; specifically, the α, C_L, C_D, and C_t magnitudes were presented according to the rotary cycles during self-start. It was found that the $\pm 180^{\circ}$ α range has a strong negative influence during the initial portion of self-start. The fluctuating α caused the coefficients to widely fluctuate, leading to specific features of the lift peaks which strongly influence C_t.As the rotor accelerated to a higher TSR, the α range began to decline, and so did the fluctuation of C_L, C_D, and C_t; yet the lift peaks remained.

Following the work by Rezaeiha *et al.,* [24], the torque coefficients and contributions were presented in a quadrant-wise breakdown, i.e., the windward, upwind, leeward, and downwind quadrants. The distribution of the generated torque according to the quadrants show that the upwind and windward quadrants generate all the initial self-starting torque while the leeward and downwind quadrants are parasitic. As the rotor reached cycle 13 (with mean TSR $= 3.6$), the roles of the quadrants changed: the downwind and windward quadrants became parasitic while the upwind and leeward quadrants generated all the torque. The data shows that this change is due to the change in α according to the quadrants, across the cycles, which results in changing C_L and C_D magnitudes, and correspondingly, altering the C_t values. Specifically, positive C_t in the quadrants was found to be due to favourable α, C_L and C_D.

Two strategies are proposed to improve rotor self-start based on the findings of this work. In essence, self-starting during the first few cycles can be improved by attempting to convert the leeward quadrants such that it mitigates the C_t dip. A key strategy could involve pitching the blades by certain angles, at the correct quadrants [43,44] or by artificially altering the tip-speed ratio to indirectly control α at specific locations, via a method called intra-cyclical control [45]. Overall, this study thus far has provided insights on the rotor dynamics to elucidate the torque performance of a Darrieus rotor during self-start, which extends the work by Celik *et al.,* [38]. A follow-up paper from this work will elucidate the physics of self-starting further by incorporating the effects of vector orientations of the forces onto the rotor dynamics.

Acknowledgement

This work was supported by Universiti Sains Malaysia (USM) through the Research University Grant Scheme (RUI.1001.PAERO.8014158).

References

[1] "EIA projects nearly 50% increase in world energy usage by 2050, led by growth in Asia," U.S. Energy Information Administration, 2019. https://www.eia.gov/todayinenergy/detail.php?id=41433

[2] "Global Wind Report 2021," 2021. https://gwec.net/global-wind-report-2021/

[3] Mertens, Sander, Gijs van Kuik, and Gerard van Bussel. "Performance of an H-Darrieus in the skewed flow on a roof." *J. Sol. Energy Eng.* 125, no. 4 (2003): 433-440. https://doi.org/10.1115/1.1629309

[4] Sharpe, Tim, and Gordon Proven. "Crossflex: Concept and early development of a true building integrated wind

turbine." *Energy and Buildings* 42, no. 12 (2010): 2365-2375. https://doi.org/10.1016/j.enbuild.2010.07.032

[5] Balduzzi, Francesco, Alessandro Bianchini, Ennio Antonio Carnevale, Lorenzo Ferrari, and Sandro Magnani. "Feasibility analysis of a Darrieus vertical-axis wind turbine installation in the rooftop of a building." *Applied Energy* 97 (2012): 921-929. https://doi.org/10.1016/j.apenergy.2011.12.008

[6] Griffith, D. Todd, Matthew F. Barone, Joshua Paquette, Brian Christopher Owens, Diana L. Bull, Carlos Simao-Ferriera, Andrew Goupee, and Matt Fowler. *Design Studies for Deep-Water Floating Offshore Vertical Axis Wind Turbines*. No. SAND2018-7002. Sandia National Lab.(SNL-NM), Albuquerque, NM (United States), 2018. https://doi.org/10.2172/1459118

[7] Blonk, D. L. "Conceptual design and evaluation of economic feasibility of floating vertical axis wind turbines." (2010).

[8] Hand, Brian, Ger Kelly, and Andrew Cashman. "Aerodynamic design and performance parameters of a lift-type vertical axis wind turbine: A comprehensive review." *Renewable and Sustainable Energy Reviews* 139 (2021): 110699. https://doi.org/10.1016/j.rser.2020.110699

[9] Lewis, Matthew, S. P. Neill, Peter Robins, M. Reza Hashemi, and Sophie Ward. "Characteristics of the velocity profile at tidal-stream energy sites." *Renewable Energy* 114 (2017): 258-272. https://doi.org/10.1016/j.renene.2017.03.096

[10] Vincent, Claire L., and Pierre-Julien Trombe. "Forecasting intrahourly variability of wind generation." In *Renewable Energy Forecasting*, pp. 219-233. Woodhead Publishing, 2017. https://doi.org/10.1016/B978-0-08-100504-0.00008-1

[11] Worasinchai, Supakit, Grant L. Ingram, and Robert G. Dominy. "The physics of H-darrieus turbines self-starting capability: flapping-wing perspective." In *Turbo Expo: Power for Land, Sea, and Air*, vol. 44724, pp. 869-878. American Society of Mechanical Engineers, 2012. https://doi.org/10.1115/GT2012-69075

[12] Hill, N., Robert Dominy, Grant Ingram, and J. Dominy. "Darrieus turbines: the physics of self-starting." *Proceedings of the Institution of Mechanical Engineers, Part A: Journal of Power and Energy* 223, no. 1 (2009): 21-29. https://doi.org/10.1243/09576509JPE615

[13] Du, Longhuan. "Numerical and experimental investigations of Darrieus wind turbine start-up and operation." PhD diss., Durham University, 2016.

[14] Dumitrescu, H., A. Dumitrache, C. L. Popescu, M. O. Popescu, F. Frunzulică, and A. Crăciunescu. "Wind tunnel experiments on vertical-axis wind turbines with straight blades." In *International conference on renewable energies and power quality*. 2014. https://doi.org/10.24084/repqj12.562

[15] Douak, M., Z. Aouachria, R. Rabehi, and N. Allam. "Wind energy systems: Analysis of the self-starting physics of vertical axis wind turbine." *Renewable and Sustainable Energy Reviews* 81 (2018): 1602-1610. https://doi.org/10.1016/j.rser.2017.05.238

[16] Zhu, Jianyang, Hailin Huang, and Hao Shen. "Self-starting aerodynamics analysis of vertical axis wind turbine." *Advances in Mechanical Engineering* 7, no. 12 (2015): 1687814015620968. https://doi.org/10.1177/1687814015620968

[17] Tahzib, Teeab, Mohammed Abdul Hannan, Yaseen Adnan Ahmed, and Iwan Zamil Mustaffa Kamal. "Performance Analysis of H-Darrieus Wind Turbine with NACA0018 and S1046 Aerofoils: Impact of Blade Angle and TSR." *CFD Letters* 14, no. 2 (2022): 10-23. https://doi.org/10.37934/cfdl.14.2.1023

[18] Beri, Habtamu, and Yingxue Yao. "Numerical simulation of unsteady flow to show self-starting of vertical axis wind turbine using fluent." *Journal of Applied Sciences* 11, no. 6 (2011): 962-970. https://doi.org/10.3923/jas.2011.962.970

[19] Asr, Mahdi Torabi, Erfan Zal Nezhad, Faizal Mustapha, and Surjatin Wiriadidjaja. "Study on start-up characteristics of H-Darrieus vertical axis wind turbines comprising NACA 4-digit series blade airfoils." *Energy* 112 (2016): 528-537. https://doi.org/10.1016/j.energy.2016.06.059

[20] Bianchini, Alessandro, Lorenzo Ferrari, and Sandro Magnani. "Start-up behavior of a three-bladed H-Darrieus VAWT: experimental and numerical analysis." In *Turbo Expo: Power for Land, Sea, and Air*, vol. 54617, pp. 811-820. 2011. https://doi.org/10.1115/GT2011-45882

[21] Sengupta, A. R., A. Biswas, and R. Gupta. "Studies of some high solidity symmetrical and unsymmetrical blade H-Darrieus rotors with respect to starting characteristics, dynamic performances and flow physics in low wind streams." *Renewable Energy* 93 (2016): 536-547. https://doi.org/10.1016/j.renene.2016.03.029

[22] Singh, M. A., A. Biswas, and R. D. Misra. "Investigation of self-starting and high rotor solidity on the performance of a three S1210 blade H-type Darrieus rotor." *Renewable energy* 76 (2015): 381-387. https://doi.org/10.1016/j.renene.2014.11.027

[23] Singh, Enderaaj, Sukanta Roy, Yam Ke San, and Law Ming Chiat. "Optimisation of H-Darrieus VAWT Solidity for Energy Extraction in Cooling Tower Exhaust Systems." *Journal of Advanced Research in Fluid Mechanics and Thermal Sciences* 91, no. 2 (2022): 51-61. https://doi.org/10.37934/arfmts.91.2.5161

[24] Abedinia, Oveis, Nima Amjady, Miadreza Shafie-Khah, and Joao PS Catalão. "Electricity price forecast using combinatorial neural network trained by a new stochastic search method." *Energy Conversion and Management* 105 (2015): 642-654. https://doi.org/10.1016/j.enconman.2015.08.025
[25] Rainbird, J. "The aerodynamic development of a vertical axis wind turbine." *Master's thesis, University of Durham, Durham, UK* (2007).
[26] Van Garrel, A. "Development of a wind turbine aerodynamics simulation module." (2003).
[27] Marten, David, Matthew Lennie, Georgios Pechlivanoglou, Christian Navid Nayeri, and Christian Oliver Paschereit. "Implementation, optimization and validation of a nonlinear lifting line free vortex wake module within the wind turbine simulation code QBlade." In *Turbo Expo: Power for Land, Sea, and Air*, vol. 56802, p. V009T46A019. American Society of Mechanical Engineers, 2015. https://doi.org/10.1115/GT2015-43265
[28] Marten, D., M. Lennie, G. Pechlivanoglou, C. D. Nayeri, and C. O. Paschereit. "Integration of an unsteady nonlinear lifting line free vortex wake algorithm in a wind turbine design framework." In *EWEA Annual Meeting*, pp. 17-20. 2015.
[29] Marten, David, Matthew Lennie, Georgios Pechlivanoglou, Christian Navid Nayeri, and Christian Oliver Paschereit. "Implementation, optimization, and validation of a nonlinear lifting line-free vortex wake module within the wind turbine simulation code qblade." *Journal of Engineering for Gas Turbines and Power* 138, no. 7 (2016). https://doi.org/10.1115/1.4031872
[30] Marten, David, Georgios Pechlivanoglou, Christian Navid Nayeri, and Christian Oliver Paschereit. "Nonlinear lifting line theory applied to vertical axis wind turbines: Development of a practical design tool." *Journal of Fluids Engineering* 140, no. 2 (2018). https://doi.org/10.1115/1.4037978
[31] Balduzzi, Francesco, David Marten, Alessandro Bianchini, Jernej Drofelnik, Lorenzo Ferrari, Michele Sergio Campobasso, Georgios Pechlivanoglou, Christian Navid Nayeri, Giovanni Ferrara, and Christian Oliver Paschereit. "Three-dimensional aerodynamic analysis of a Darrieus wind turbine blade using computational fluid dynamics and lifting line theory." *Journal of Engineering for Gas Turbines and Power* 140, no. 2 (2018). https://doi.org/10.1115/1.4037750
[32] Bianchini, Alessandro, David Marten, Andrea Tonini, Francesco Balduzzi, Christian Navid Nayeri, Giovanni Ferrara, and Christian Oliver Paschereit. "Implementation of the "virtual camber" transformation into the open source software QBlade: validation and assessment." *Energy Procedia* 148 (2018): 210-217. https://doi.org/10.1016/j.egypro.2018.08.070
[33] Marten, D., G. Pechlivanoglou, C. N. Nayeri, and C. O. Paschereit. "Integration of a WT Blade Design tool in XFOIL/XFLR5." In *10th German Wind Energy Conference (DEWEK 2010), Bremen, Germany, Nov*, pp. 17-18. 2010.
[34] Montgomerie, Björn. "Methods for root effects, tip effects and extending the angle of attack range to {+-} 180 deg., with application to aerodynamics for blades on wind turbines and propellers." (2004).
[35] Leishman, J. Gordon, and T. S. Beddoes. "A Semi-Empirical model for dynamic stall." *Journal of the American Helicopter society* 34, no. 3 (1989): 3-17. https://doi.org/10.4050/JAHS.34.3.3
[36] Himmelskamp, H. *Profile investigations on a rotating airscrew*. Ministry of Aircraft Production, 1947.
[37] Marten, David, Alessandro Bianchini, Georgios Pechlivanoglou, Francesco Balduzzi, Christian Navid Nayeri, Giovanni Ferrara, Christian Oliver Paschereit, and Lorenzo Ferrari. "Effects of Airfoil's Polar Data in the Stall Region on the Estimation of Darrieus Wind Turbine Performance." In *Turbo Expo: Power for Land, Sea, and Air*, vol. 49873, p. V009T46A007. American Society of Mechanical Engineers, 2016. https://doi.org/10.1115/GT2016-56685
[38] Celik, Yunus, Lin Ma, Derek Ingham, and Mohamed Pourkashanian. "Aerodynamic investigation of the start-up process of H-type vertical axis wind turbines using CFD." *Journal of Wind Engineering and Industrial Aerodynamics* 204 (2020): 104252. https://doi.org/10.1016/j.jweia.2020.104252
[39] Schmitz, Sven, and Jean-Jacques Chattot. "Characterization of three-dimensional effects for the rotating and parked NREL Phase VI wind turbine." (2006): 445-454. https://doi.org/10.1115/1.2349548
[40] Arab, A., M. Javadi, M. Anbarsooz, and M. Moghiman. "A numerical study on the aerodynamic performance and the self-starting characteristics of a Darrieus wind turbine considering its moment of inertia." *Renewable Energy* 107 (2017): 298-311. https://doi.org/10.1016/j.renene.2017.02.013
[41] Hill, N., Robert Dominy, Grant Ingram, and J. Dominy. "Darrieus turbines: the physics of self-starting." *Proceedings of the Institution of Mechanical Engineers, Part A: Journal of Power and Energy* 223, no. 1 (2009): 21-29. https://doi.org/10.1243/09576509JPE615
[42] Baker, J. R. "Features to aid or enable self starting of fixed pitch low solidity vertical axis wind turbines." *Journal of Wind Engineering and Industrial Aerodynamics* 15, no. 1-3 (1983): 369-380. https://doi.org/10.1016/0167-6105(83)90206-4
[43] Somoano, M., and F. J. Huera-Huarte. "The dead band in the performance of cross-flow turbines: Effects of Reynolds number and blade pitch." *Energy Conversion and Management* 172 (2018): 277-284. https://doi.org/10.1016/j.enconman.2018.06.087

[44] Zouzou, B., Ivan Dobrev, Fawaz Massouh, and Rabah Dizene. "Experimental and numerical analysis of a novel Darrieus rotor with variable pitch mechanism at low TSR." *Energy* 186 (2019): 115832. https://doi.org/10.1016/j.energy.2019.07.162

[45] Strom, Benjamin, Steven L. Brunton, and Brian Polagye. "Intracycle angular velocity control of cross-flow turbines." *Nature Energy* 2, no. 8 (2017): 1-9. https://doi.org/10.1038/nenergy.2017.103

[46] Mahrous, Abdel-Fattah. "A Computational Fluid Dynamics Study of an Integrating Savonius-Darrieus Vertical Axis Wind Turbine." *Journal of Advanced Research in Fluid Mechanics and Thermal Sciences* 75, no. 1 (2020): 21-37. https://doi.org/10.37934/arfmts.75.1.2137